http://www.jstage.jst.go.jp/browse/biophysics

BIOPHYSICS

Vol. 10, pp. 109–119 (2014)
doi: 10.2142/biophysics.10.109

Microscopic heat pulse-induced calcium dynamics in single WI-38 fibroblasts

Hideki Itoh[1,2], Kotaro Oyama[3], Madoka Suzuki[4,5] and Shin'ichi Ishiwata[1,3,4,5]

[1]*Department of Pure and Applied Physics, Graduate School of Advanced Science and Engineering, Waseda University, 3-4-1 Okubo, Shinjuku-ku, Tokyo 169-8555, Japan*
[2]*Institute of Medical Biology, Agency for Science Technology & Research (A*STAR), 8A Biomedical Grove, #06-06 Immunos, Singapore 138648, Singapore*
[3]*Department of Physics, Faculty of Advanced Science and Engineering, Waseda University, 3-4-1 Okubo, Shinjuku-ku, Tokyo 169-8555, Japan*
[4]*Waseda Bioscience Research Institute in Singapore (WABIOS), 11 Biopolis Way, #05-02 Helios, Singapore 138667, Singapore*
[5]*Organization for University Research Initiatives, Waseda University, 513 Waseda Tsurumaki-cho, Shinjuku-ku, Tokyo 162-0041, Japan*

Received September 17, 2014; accepted November 16, 2014

Temperature-sensitive Ca^{2+} dynamics occur primarily through transient receptor potential channels, but also by means of Ca^{2+} channels and pumps on the endoplasmic reticulum membrane. As such, cytoplasmic Ca^{2+} concentration ($[Ca^{2+}]_{cyt}$) is re-equilibrated by changes in ambient temperature. The present study investigated the effects of heat pulses (heating duration: 2 s or 150 s) on $[Ca^{2+}]_{cyt}$ in single WI-38 fibroblasts, which are considered as normal cells. We found that Ca^{2+} burst occurred immediately after short (2 s) heat pulse, which is similar to our previous report on HeLa cells, but with less thermosensitivity. The heat pulses originated from a focused 1455-nm infrared laser light were applied in the vicinity of cells under the optical microscope. Ca^{2+} bursts induced by the heat pulse were suppressed by treating cells with inhibitors for sarco/endoplasmic reticulum Ca^{2+} ATPase (SERCA) or inositol trisphosphate receptor (IP_3R). Long (150 s) heat pulses also induced Ca^{2+} bursts after the onset of heating and immediately after re-cooling. Cells were more thermosensitive at physiological (37°C) than at room (25°C) temperature; however, at 37°C, cells were responsive at a higher temperature (ambient temperature+heat pulse). These results strongly suggest that the heat pulse-induced Ca^{2+} burst is caused by a transient imbalance in Ca^{2+} flow between SERCA and IP_3R, and offer a potential new method for thermally controlling Ca^{2+}-regulated cellular functions.

Key words: calcium imaging, ER, IR laser, temperature change, thermometer sheet

Corresponding authors: Shin'ichi Ishiwata, Department of Physics, Faculty of Advanced Science and Engineering, Waseda University, 3-4-1 Okubo, Shinjuku-ku, Tokyo 169-8555, Japan. e-mail: ishiwata@waseda.jp; Madoka Suzuki, Waseda Bioscience Research Institute in Singapore (WABIOS), 11 Biopolis Way, #05-02 Helios, Singapore 138667, Singapore. e-mail: suzu_mado@aoni.waseda.jp

The activity of many Ca^{2+}-associated proteins is temperature-dependent. Most prominent among these are transient receptor potential channels (TRP channels), which function as sensors that are activated when the ambient temperature is either above (V1, V2, V3, and V4) or below (M8 and A1) a critical temperature[1]. Other examples include Ca^{2+} channels located at the endoplasmic reticulum (ER) membrane, ryanodine receptor (RyR), and inositol trisphosphate receptor (IP_3R). The probability of these channels opening, i.e., the open probability, increases with decreasing temperature[2–6]. The Ca^{2+} pump located at ER membrane—sarco/endoplasmic reticulum Ca^{2+} ATPase (SERCA)—is also thermosensitive, with the ATPase activity increasing as a function of temperature[7].

Cytoplasmic Ca^{2+} concentration ($[Ca^{2+}]_{cyt}$) at any given temperature is the sum of the temperature-dependent activities of these channels. When temperature changes, the overall $[Ca^{2+}]_{cyt}$ response (the time course of $[Ca^{2+}]_{cyt}$) becomes complex, and may even be destabilized. In human keratinocytes,

$[Ca^{2+}]_{cyt}$ increases as a function of temperature (from 30°C to 50°C over 40 s), possibly due to the activity of TRP channels[8]. In insect cells, $[Ca^{2+}]_{cyt}$ increases during tissue freezing (from 25°C to 0°C over 25 min) due to the inhibition of the Na/K ATPase and SERCA[9]. We also reported on the Ca^{2+} dynamics of HeLa cells[6]; transient alterations in $[Ca^{2+}]_{cyt}$ were detected at 37°C in response to single heat pulses with a temperature change of 0.2°C or greater, where both heating and re-cooling were achieved in less than 100 ms. These highly thermosensitive $[Ca^{2+}]_{cyt}$ dynamics were attributable to the altered balance between Ca^{2+} uptake by SERCA and Ca^{2+} bursts through IP_3R.

In the present study, the response of single WI-38 fibroblasts—considered as normal cells[10–13]—to thermal stimuli delivered by means of heat pulses was investigated. The results demonstrate that Ca^{2+} bursts depend on both ambient temperature and temperature changes induced by microscopic heat pulses.

Materials and Methods

Cell culture

Human lung embryonic WI-38 fibroblasts (Human Science Research Resource Bank, Osaka, Japan) were maintained and subcultured to 35–50 population doubling level in minimum essential medium (MEM; Thermo Fisher Scientific, MA, USA) supplemented with 10% fetal bovine serum (FBS; Thermo Fisher Scientific) and 200 U/mL penicillin G sodium salt (Sigma-Aldrich, MO, USA). For functional experiments, cells were cultured overnight in a 35 mm-glass base dish (No. 3911-035, AGC TECHNO GLASS, Shizuoka, Japan) at 37°C and 5% CO_2.

Microscopy

The microscope was similar to the one that was previously used[14]. An IX70 inverted microscope with a PlanApo N 60×/1.45 oil objective lens (Olympus, Tokyo, Japan) was mounted on an optical bench. A mercury lamp and Lambda 10-3 filter wheel (Sutter Instrument, CA, USA) were set outside the bench and connected to the microscope via a liquid light guide. To prevent excessive bleaching of the fluorescence signal, neutral density filters were placed in front of a liquid light guide. Fluorescence images were recorded with BP360-370, DM505, and BA515IF (respectively, excitation filter, dichroic mirror, and emission filter) for thermometer sheet; BP470-490, DM505, and BA515IF (a green channel) for Ca^{2+} dynamics; BP520-550, FF562-Di02, and BA580IF (a red channel) for injection marker, respectively (FF562-Di02, Semrock, NY, USA; others, Olympus). For bright field and fluorescence imaging, an iXon EM+ 897 electron multiplying charge-coupled device camera shooting an average of 9.9 frames/s and Andor iQ software (Andor Technology, Antrim, UK) were used along with an FF01-790 short-pass filter (Semrock) placed in front of the camera.

Ambient temperature control

Ambient temperature was maintained at 24.9±0.4°C or 36.6±0.5°C (measurement error: ±1°C) for room and physiological temperatures, respectively, by a KRi stage top incubator (Tokai Hit, Shizuoka, Japan). In experiments studying the effects of heating duration, the ambient temperature was set at 26.5°C without using the stage top incubator.

Microscopic heating system

Heat pulses were delivered to WI-38 fibroblasts by focusing an infrared laser (IR laser; λ=1455 nm, KPS-STD-BT-RFL-1455-02-CO, Keopsys, Côtes-d'Armor, France) on a region next to the cells[14,15] and directly heating the HEPES-buffered saline solution (HEPES-BSS; 134 mM NaCl, 5.4 mM KCl, 1.0 mM $MgSO_4$, 1.0 mM NaH_2PO_4, 1.8 mM $CaCl_2$, 20 mM HEPES, and 5 mM D-glucose, adjusted to pH 7.4 by adding NaOH) containing 10% FBS. Cells were not directly irradiated to eliminate the immediate effects of light. The on/off heating control was regulated by an SSH-C4B shutter system (Sigma Koki, Saitama, Japan) placed in the light path of the IR laser. Values given for laser power were those displayed on the controller of the IR laser device.

Thermometer sheet

A glass-bottom dish was placed at the bottom of a small centrifuge (Tomy Seiko, Tokyo, Japan), and a mixture containing 8 μL of 10 mg/mL Europium (III) thenoyltrifluoroacetonate trihydrate (Eu-TTA; Thermo Fisher Scientific) in acetone and 8 μL of 20 mg/mL poly(methyl methacrylate) (PMMA; MW=15,000; Sigma-Aldrich) in acetone was added dropwise to the center of the dish. Immediately afterwards, the dish was spin-coated over 10 s and dried at room temperature. The thermometer sheet on the dish was filled with 2 mL HEPES-BSS and imaged by fluorescence microscopy. Images were analyzed using ImageJ software (National Institutes of Health, MD, USA). The fluorescence intensity of the thermometer sheet 1 s after the start of IR laser irradiation was normalized to the mean fluorescence intensity 1 s before the start of irradiation. ΔT in each camera pixel was then calculated using the calibration curve (Supplementary Fig. S1). Lastly, ΔT as a function of the distance d (in μm) between the center of the IR laser focal point and the centroid of the cell was fitted using the following formula: $\Delta T = -C_1 \ln(d/d_0) + C_2$, where $C_1 > 0$, $C_2 > 0$, and $d_0 = 1$ (in μm) (Table 1).

Ca^{2+} imaging

WI-38 fibroblasts cultured in MEM were rinsed twice with 1 mL HEPES-BSS without FBS, and incubated in 200 μL of 5 μM fluo-4, AM (Thermo Fisher Scientific, 0.5% dimethyl sulfoxide (DMSO)) in HEPES-BSS without FBS for 20 min at room temperature. At indicated time points, cells were treated with the following chemical reagents: 5 mM Ethylene glycol tetraacetic acid (EGTA; Dojindo Laboratories, Kumamoto, Japan) only during the measurement; 2 μM thap-

Table 1 Summary of ΔT gradient formulae at various levels of IR laser power

Laser power (W)	ΔT gradient at 25°C (°C)	ΔT gradient at 37°C (°C)
3.09×10^{-1}	$-0.668\ \ln(d/d_0)+4.57$	$-0.604\ \ln(d/d_0)+4.13$
7.41×10^{-1}	$-1.76\ \ln(d/d_0)+11.6$	$-1.48\ \ln(d/d_0)+9.84$
1.20	$-2.91\ \ln(d/d_0)+19.2$	$-2.23\ \ln(d/d_0)+15.2$
1.66	$-3.93\ \ln(d/d_0)+26.0$	$-2.83\ \ln(d/d_0)+19.6$
2.14	$-4.79\ \ln(d/d_0)+32.1$	$-3.38\ \ln(d/d_0)+23.6$

Laser power values were those displayed on the controller. Square ROIs (n=51) were set as 5.38 μm×5.38 μm. ΔT gradients were measured three times at 25°C or twice at 37°C. d (in μm) is defined as the distance from the IR laser focal point to the center of the ROI. The unit in the logarithm was cancelled by setting d_0=1 (in μm).

sigargin (Merck KGaA, Darmstadt, Germany) for the 30-min pre-treatment and during the measurement (0.1% DMSO); 25 μM ryanodine (Wako Pure Chemical Industries, Osaka, Japan) for the 30-min pre-treatment and during the measurement; 27 mg/mL heparin (Merck KGaA) and 0.1 mg/mL tetramethylrhodamine-dextran (TMR-dextran; MW=10,000; Thermo Fisher Scientific) in injection buffer (140 mM KCl, 2 mM $MgCl_2$, and 10 mM HEPES adjusted to pH 7.4 by adding KOH) injected to the cells before fluo-4 staining; 0.1 mg/mL TMR-dextran in injection buffer injected to the cells before fluo-4 staining for injection control; 5, 10, 50, 100, 200, or 500 μM 2-aminoethoxydiphenyl borate (2-APB; Sigma-Aldrich) only during the measurement (0.5% DMSO for 500 μM, 0.2% DMSO for 200 μM, and 0.1% for other concentrations). Fluo-4, AM-loaded cells were rinsed twice with 1 mL HEPES-BSS without FBS, cultured in 2 mL HEPES-BSS, and transferred to the microscope stage where they were left undisturbed for at least 10 min until the temperature had stabilized. One single cell or at most two single cells were observed within the field of view in most of the measurements. All measurements were repeated with multiple culture dishes in each condition. Images of fluo-4 fluorescence were analyzed by ImageJ. Each region of interest (ROI) was manually traced in bright field images to cover a whole cell. In order to determine the level of fluorescent cross-talk between fluo-4 and TMR-dextran, the intensity of TMR-dextran injected cells (without fluo-4) was plotted as a ratio of the green channel against the red channel. The background intensity obtained from this was then subtracted from the intensity of cells injected with TMR-dextran in the presence of fluo-4. The data were smoothed by a moving average with a window size of five data points. The $\Delta F_{max}/F_0$ was defined as the maximum $\Delta F/F_0$ within 15 s of re-cooling. The $\Delta F_{min}/F_0$ was defined as the minimum $\Delta F/F_0$ during heating. The peak time of the Ca^{2+} burst was defined as the time of the maximum fluorescence intensity observed in the measurements after re-cooling.

Statistical analysis

All statistical analyses were performed with Microsoft Excel (Microsoft, WA, USA), OriginPro 8.5 (OriginLab, Northampton, MA, USA), or EZR (Saitama Medical Center, Jichi Medical University, Saitama, Japan), which is a graphical user interface for R (The R Foundation for Statistical Computing, Vienna, Austria). P values were calculated with the Mann-Whitney U or F tests as indicated. Significant differences $0.01\leq p<0.05$ and $p<0.01$ are denoted by single and double asterisks in the figures, respectively.

Results

Delivery of a microscopic heat pulse via IR laser

A microscopic heat pulse was delivered using a 1455-nm IR laser light (Fig. 1A). As the laser light is absorbed by water, the focal point becomes a heat source around which a radial temperature gradient is created in the X-Y plane[15] (Fig. 1B, C; Supplementary Movie S1). The temperature distribution was visualized by means of a thermometer sheet consisting of a thin layer of PMMA doped with the thermosensitive fluorophore Eu-TTA on the upper surface of glass-bottom dishes. Since the fluorescence intensity of Eu-TTA decreases with increasing temperature[16,17], the thermometer sheet was calibrated with a stage top incubator to convert the change in fluorescence intensity into a temperature change ΔT (–2.8%/°C relative to 25°C) (Supplementary Fig. S1). The temperature distribution delivered by the IR laser light reached 63% (i.e., $1-e^{-1}$) of the maximum value within approximately 0.1 s of closing or opening the shutter located in the laser light path (Fig. 1D). Also, ΔT can be controlled by the laser power and the distance from the heat source (Fig. 1C, D; Table 1).

Ca^{2+} bursts are induced by a single microscopic heat pulse

A cytoplasmic Ca^{2+} burst was observed in a WI-38 fibroblast exposed to a heat pulse (Fig. 2A; Supplementary Movie S2). Isolated single cells were tested to avoid activating ATP-mediated chemical signaling[18,19] and/or direct cell-cell communication through gap junctions[18–20]. The Ca^{2+} burst started immediately after re-cooling, reaching a peak $\Delta F_{max}/F_0$ of 1.1±0.9 (mean±standard deviation) (Fig. 2G) within about 10 s before $[Ca^{2+}]_{cyt}$ returned to the pre-pulse level.

Ca^{2+} bursts persisted in the presence of 5 mM EGTA in Ca^{2+}-free HEPES-BSS (Fig. 2B). The $\Delta F_{max}/F_0$ was 0.72±0.79, which was not significantly different from the value in untreated cells (Fig. 2G). Next, Ca^{2+} influx and efflux via ER, an intracellular Ca^{2+} store, were suppressed (Fig. 2C–E). After

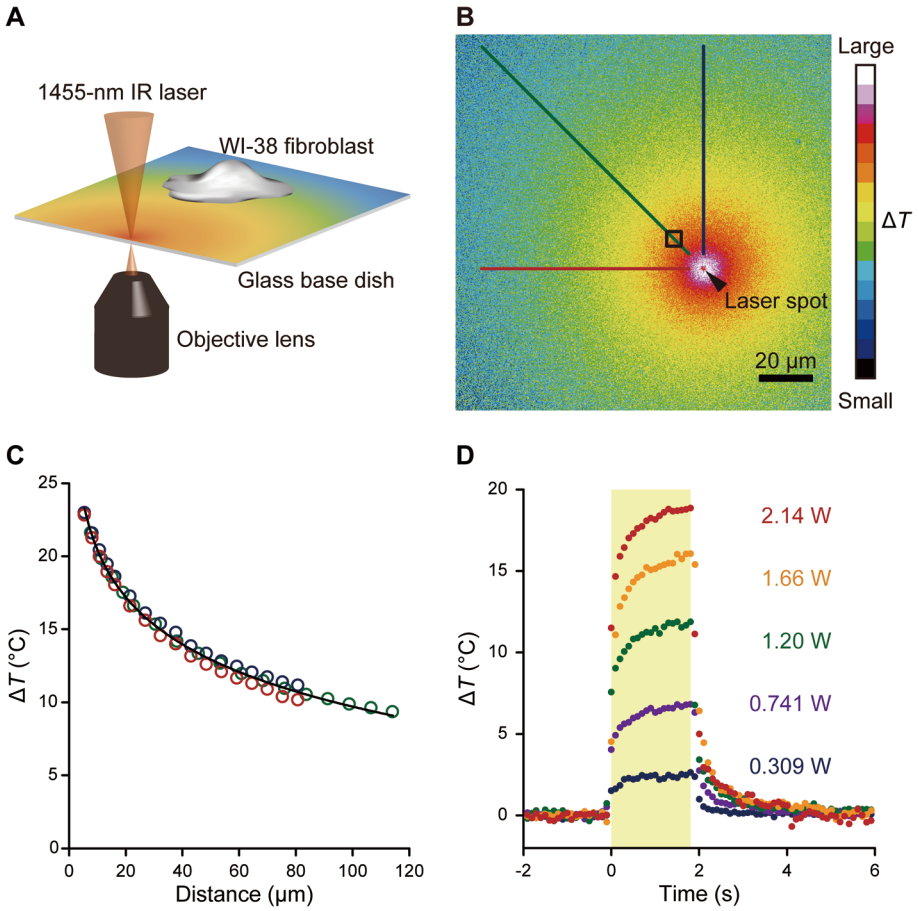

Figure 1 Quantification of a heat pulse induced by a focused 1455-nm IR laser using a fluorescent thermometer sheet. (A) Schematic illustration of the microscopic heating system. A local temperature gradient was induced by focusing an IR laser (1455 nm). (B) Representative image of the X-Y distribution of ΔT imaged on a thermometer sheet at 25°C. The laser power displayed on the controller was 2.14 W. Scale bar, 20 μm. A black arrowhead indicates the focal point of the IR laser. An accompanying movie is available (Supplementary Movie S1). (C) ΔT distribution in three different directions from the heat source in (B) is indicated by lines. Plots were obtained from lines with the same color code. Black curve, ΔT against the distance from the IR laser spot (d in μm), is the fitted curve using ΔT=−4.64 ln(d/d_0)+31.1, where d_0=1 (in μm). Calibration curves at other laser powers are shown in Table 1. (D) Time course of ΔT in the ROI indicated by a black square in (B) for each laser power (0.309, 0.741, 1.20, 1.66, and 2.14 W, as displayed on the controller). A yellow area represents the duration of IR laser irradiation.

a 30-min pretreatment of cells with 2 μM thapsigargin, a SERCA inhibitor, Ca^{2+} in ER is supposed to be depleted, and $\Delta F_{max}/F_0$ decreased to 0.20±0.16 (Fig. 2C, G). Blocking SERCA by thapsigargin results in Ca^{2+} store depletion as well as an activation of store-operated Ca^{2+} channels, and thus may initially lead to an elevated $[Ca^{2+}]_{cyt}$. However, as consistent with Maloney *et al.*'s study[21], we confirmed that the steady state F_0 values showed no significant difference between thapsigargin-treated (for 30 min) and untreated cells (Supplementary Fig. S2). Cells pretreated for 30 min with 25 μM ryanodine, an RyR inhibitor, showed Ca^{2+} bursts as large as $\Delta F_{max}/F_0$=1.7±1.3 (Fig. 2D, G). Then, we focused on IP_3R. Injection of 27 mg/mL heparin significantly weakened the response to a heat pulse ($\Delta F_{max}/F_0$=0.25±0.18) (Fig. 2E, G), whereas injection control remained responsive ($\Delta F_{max}/F_0$=1.9±1.7) (Fig. 2F, G). We further confirmed that 2-APB, which is also known as an inhibitor of IP_3R, reduced the response in a dose-dependent manner (Fig. 2H).

We examined the Ca^{2+} dynamics during heating (Fig. 3). First, the time course in thapsigargin-treated cells was considerably different from other conditions (Fig. 3A). Second, the minimum peak value during heating ($\Delta F_{min}/F_0$) was the least in thapsigargin-treated cells (Fig. 3B). According to Figures 2 and 3, we conclude that ER—specifically, SERCA activity and IP_3R state—is involved in heat pulse-induced Ca^{2+} bursts.

Peak time of Ca^{2+} bursts varies as a function of heating duration

Our previous study on HeLa cells suggested that a heat pulse produces an imbalance of net Ca^{2+} flow via ER membrane due to differences in thermosensitivity between SERCA and IP_3R, thereby inducing Ca^{2+} bursts[6]; the present results suggest a similar mechanism in WI-38 fibroblasts. To

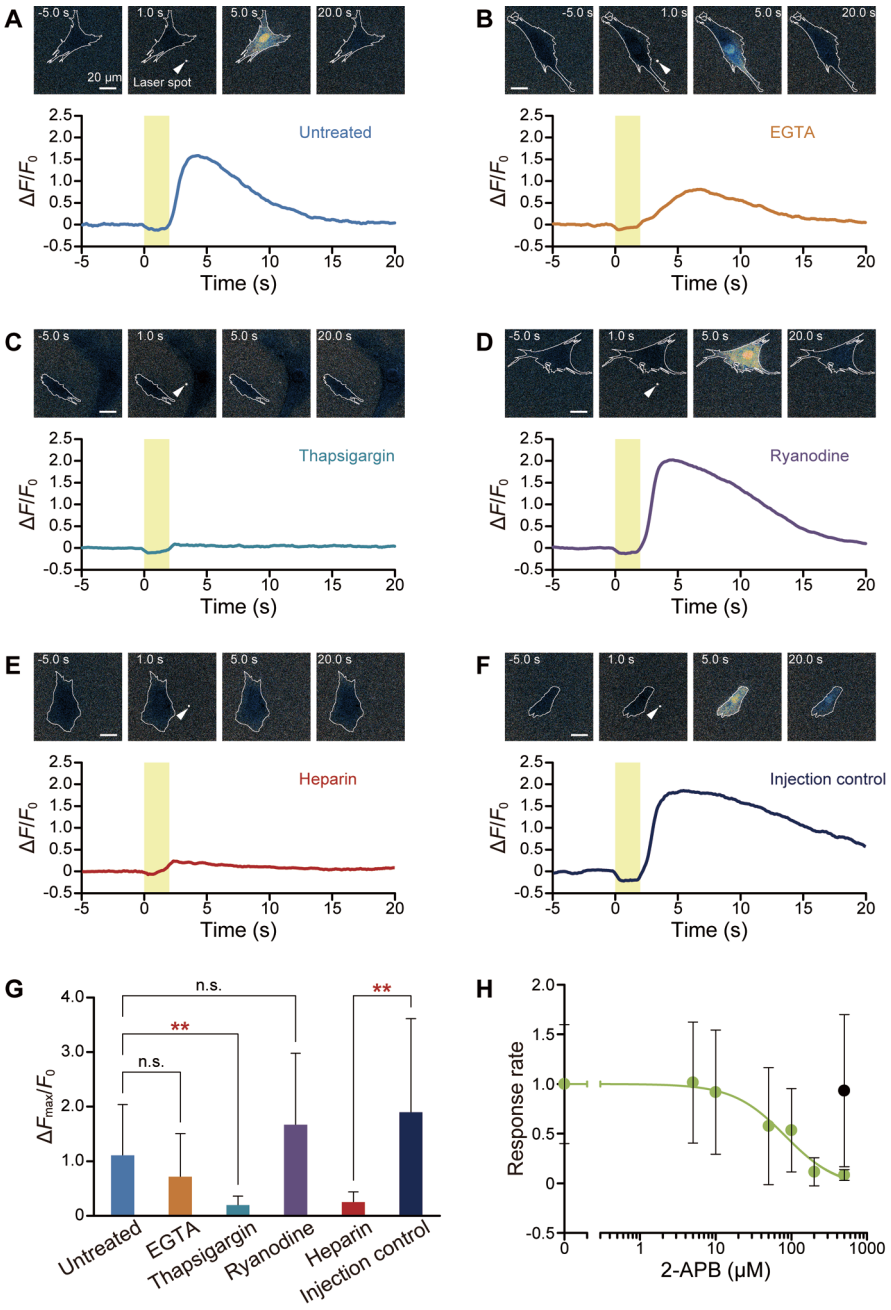

Figure 2 ER as the major Ca^{2+} source. (A–F) Representative images and time course of fluo-4 fluorescence in an untreated cell (A), and in cells treated with 5 mM EGTA (B), 2 μM thapsigargin (C), 25 μM ryanodine (D), 27 mg/mL heparin (E), and injection control (F). Yellow areas represent the duration of IR laser irradiation. White arrowheads indicate the focal points of the IR laser. Scale bars, 20 μm. Cell borders are traced with white lines. (G) Comparison of $\Delta F_{max}/F_0$ in untreated cells (n=14 cells, ΔT=13.9±0.9°C (mean±standard deviation)), or cells treated with 5 mM EGTA (n=17 cells, ΔT=14.0±1.0°C), 2 μM thapsigargin (n=15 cells, ΔT=13.6±1.0°C), 25 μM ryanodine (n=16 cells, ΔT=13.8±0.9°C), 27 mg/mL heparin (n=13 cells, ΔT=14.5±1.0°C), or injection control (n=19 cells, ΔT=15.5±0.7°C). Data represent mean±standard deviation. Each dataset was compared to untreated cells (EGTA, p=0.16; thapsigargin, $p=1.3\times10^{-3}$; ryanodine, p=0.38) or to injection control (heparin, $p=2.2\times10^{-3}$). Significant differences ($p<0.01$) are indicated by double asterisks. (H) Dose-response curve against 2-APB for 0 (n=20 cells, ΔT=14.8±0.7°C), 5 (n=21 cells, ΔT=14.9±0.8°C), 10 (n=21 cells, ΔT=14.8±0.6°C), 50 (n=21 cells, ΔT=14.9±0.6°C), 100 (n=23 cells, ΔT=14.8±0.8°C), 200 (n=17 cells, ΔT=14.5±0.9°C), or 500 (n=16 cells, ΔT=15.2±0.7°C, green plot) μM. Black plot at 500 μM indicates a 0.5% DMSO control without 2-APB (n=19 cells, ΔT=14.8±0.5°C). DMSO concentrations were 0.5% in 500 μM 2-APB, 0.2% in 200 μM 2-APB, or 0.1% in other conditions. The response rates were calculated as the value relative to 0 μM 2-APB (0.1% DMSO). The plots represent mean±standard deviation and the green curve is the fitted curve using $y=-0.044+\frac{1+0.044}{1+(x/83)^{1.3}}$, where x and y are the concentration of 2-APB (μM) and the response rate, respectively. The p value between 0.1% and 0.5% DMSO (both 2-APB free) is 0.71. IC_{50} was 83 μM. The laser power displayed on the controller was 2.14 W. Data at each time point were normalized by the average value for 5 s before heating (F_0).

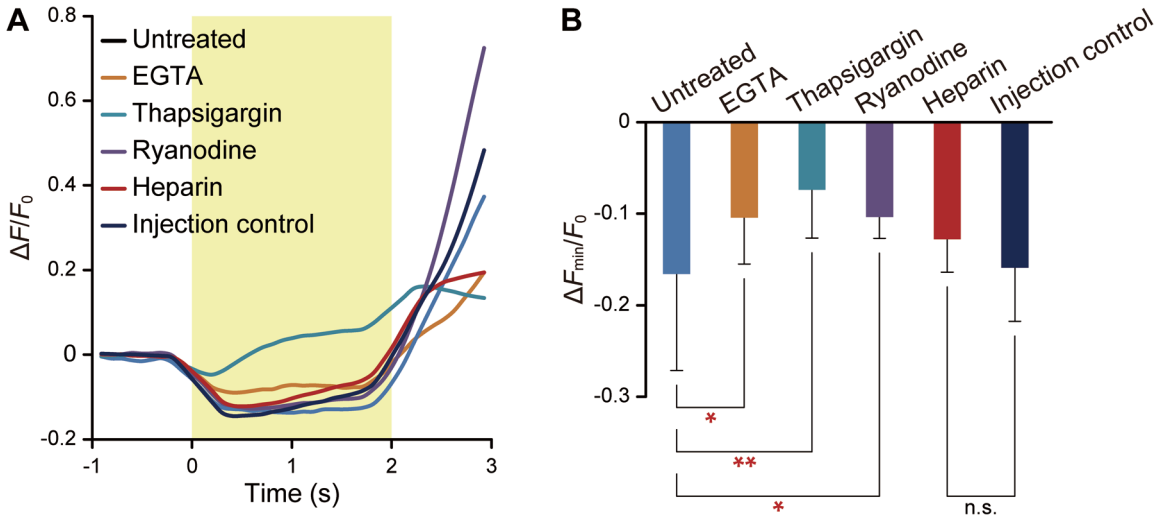

Figure 3 Heat pulse-accelerated Ca^{2+} influx from cytoplasm to ER via SERCA. (A) Average time course of $\Delta F/F_0$ in untreated (n=14 cells, ΔT=13.9±0.9°C) and in cells treated with 5 mM EGTA (n=17 cells, ΔT=14.0±1.0°C), 2 μM thapsigargin (n=15 cells, ΔT=13.6±1.0°C), 25 μM ryanodine (n=16 cells, ΔT=13.8±0.9°C), 27 mg/mL heparin (n=13 cells, ΔT=14.5±1.0°C), and injection control (n=19 cells, ΔT=15.5±0.7°C). The duration of irradiation is indicated by the yellow area. (B) Comparison of $\Delta F_{min}/F_0$. Data represent mean±standard deviation. Each dataset was compared to untreated cells (EGTA, $p=3.2\times10^{-2}$; thapsigargin, $p=5.2\times10^{-4}$; ryanodine, p=0.01) or to injection control (heparin, p=0.16). Significant differences $0.01\leq p<0.05$ and $p<0.01$ are indicated by single and double asterisks, respectively. Data at each time point were normalized by the average value for 5 s before heating (F_0).

further examine this mechanism, short (2 s) or long (150 s) heat pulses were applied (Fig. 4A, B, respectively). To compare the $\Delta F_{max}/F_0$ after pulses of different durations, taking into account the photobleaching of fluo-4 fluorescence during the measurements, short heat pulses were applied at 148 s as shown in Figure 4A. Some of the $\Delta F_{max}/F_0$ shown in Figure 4A and B have negative values on average. It was probably due to the F_0 which were average fluorescence intensities from −5 s to 0 s taken during the spontaneous Ca^{2+} release phase. Two kinds of Ca^{2+} bursts were induced by long heat pulses (Fig. 4B). After the onset of heating, $[Ca^{2+}]_{cyt}$ initially decreased and then increased, which was followed by a dampening of $[Ca^{2+}]_{cyt}$ oscillation. On the other hand, after re-cooling at the end of the long heat pulse, Ca^{2+} burst occurred; in this case, $\Delta F_{max}/F_0$ (0.81±0.56) was comparable to the value obtained with a short pulse (0.83±0.86) (Fig. 4C). However, the peak time, the timing of the Ca^{2+} burst after re-cooling, in long pulses (3.3±1.3 s) was significantly shorter than that of the first Ca^{2+} burst after the onset of long heating (16.5±5.7 s) (Fig. 4D). Furthermore, the peak time of the Ca^{2+} burst after a long pulse was markedly shorter and more sharply distributed (F-test: $p=9.3\times10^{-10}$) than after a short pulse (9.2±8.5 s) (Fig. 4D).

WI-38 fibroblasts have greater thermosensitivity at 37°C than at 25°C

Various ΔT (temperature difference against ambient temperature) stimuli were examined in WI-38 fibroblasts at room and physiological temperatures (25°C and 37°C, respectively) (Fig. 5; Supplementary Fig. S3). As the dissociation constant (K_d) of fluo-4 in the presence of Ca^{2+} decreases with increases in temperature, the fluorescence intensities of fluo-4 at different temperatures are not quantitatively comparable[22]. However, it was also reported that the $\Delta F/F_0$ of a BAPTA-based probe is stable upon changes in temperature except at high intensities ($\Delta F/F_0>6$)[5,23]. In this study, $\Delta F/F_0$ was no greater than ~3, and therefore Ca^{2+} bursts were compared by means of $\Delta F/F_0$ at different ambient temperatures. Cells responded to ΔT between 4.4°C and 7.5°C at 37°C as compared to 7.7°C and 10.7°C at 25°C (Fig. 5A, B). At both ambient temperatures, $\Delta F_{max}/F_0$ increased at greater ΔT once $\Delta F_{max}/F_0$ reached the threshold ΔT although the $\Delta F_{max}/F_0$ values among cells were varied (Supplementary Fig. S3). Previously, similar trends were observed in HeLa cells[6]. At the same ΔT, $\Delta F_{max}/F_0$ was larger in cells at 37°C than at 25°C; however, when $\Delta F_{max}/F_0$ was replotted against T= ambient temperature+ΔT, cells at 25°C showed a response over around 33°C, i.e., below 37°C (Fig. 5C).

Discussion

Thermometer sheets have previously been employed to image the heterogeneous temperature distribution in integrated circuits under dry conditions[17]. In the present study, this method was used to image temperature in aqueous conditions. We have reported on other methods of microscopic thermometry such as the thermometer micropipette[16] and nanothermometer probes[24,25]. Although the change in fluorescence intensity of Eu-TTA can be precisely measured by these methods, they monitor temperature changes only at the

places of the micropipette tip or probe. The thermometer sheet has some distinct advantages: first, a two-dimensional temperature map can be drawn (Fig. 1B); second, a temperature map can be obtained from one of the largest surfaces, i.e., the glass coverslip to which cells adhere.

Ca^{2+} bursts were induced in WI-38 fibroblasts by smaller ΔT at physiological (37°C) as compared to room (25°C) temperature. This was consistent with our previous results in HeLa cells, which are a cancer cell line[6]. We also reported that adult rat cardiomyocytes contract without Ca^{2+} transients during heating, where a similar heat pulse-induced contraction was generated by a smaller ΔT at physiological than at room temperature[14]. Here, we found that WI-38 fibroblasts responded to the heat pulse in a similar manner to the cells studied previously, but WI-38 fibroblasts were less thermosensitive (Fig. 5; Supplementary Fig. S3).

Our results suggest a plausible model of the molecular mechanism for heat pulse-induced Ca^{2+} bursts in WI-38 fibroblasts (Fig. 6), which includes the following steps. In a short heat pulse, (i) the net flow of Ca^{2+} across ER membrane is zero, i.e., a steady state, at any temperature unless cells are stimulated, for instance, by an influx of Ca^{2+} into cytoplasm via TRPM7, which is a stretch-activated Ca^{2+} channel located at cell membrane[26]. (ii) With increasing temperature, the net Ca^{2+} flow rapidly shifts towards ER due to increased SERCA activity[6,7] and decreased open probability of IP_3R[3,5,6]. (iii) The latter increases instantaneously after re-cooling, which is followed by Ca^{2+}-induced Ca^{2+} release (CICR)[3,5,6]. Figures 5 and S3 show varied responses (in other words, large standard deviations) even at greater ΔT, probably because some cells can reach the threshold of CICR and others cannot as observed in neurons[27]. (iv) The excess cytoplasmic Ca^{2+} activates SERCA[28,29] and switches IP_3R to the closed state due to the bell-shaped dependence of IP_3R open probability on $[Ca^{2+}]_{cyt}$[30]; i.e., the open probability of IP_3R is the highest in the mid-range of $[Ca^{2+}]_{cyt}$ (100 nM–1 μM), and lower above or below this range[31]. (v) $[Ca^{2+}]_{cyt}$ is then restored to the original level and total Ca^{2+} flow through ER membrane returns to zero.

In a long heat pulse, (i) is the same as for a short heat pulse. (ii-a) Heating initially accelerates SERCA activity[7] while decreasing the open probability of IP_3R[3,5,6]. (ii-b) It is shown that Ca^{2+} concentration inside ER ($[Ca^{2+}]_{ER}$) at a steady state is maintained constant at 22°C and 37°C in HeLa cells[32,33]. The outflow of Ca^{2+} from ER to cytoplasm through IP_3R is increased to maintain a certain $[Ca^{2+}]_{ER}$. In the meantime, SERCA activity is gradually suppressed due to greater differences between $[Ca^{2+}]_{cyt}$ and $[Ca^{2+}]_{ER}$. (iii) The probability of a large Ca^{2+} outflow from ER to cytoplasm through IP_3R is increased by passive transport, so that CICR occurs suddenly when $[Ca^{2+}]_{cyt}$ near IP_3R reaches a level that is sufficient to induce IP_3R opening[30,31]. Steps (ii-b) and (iii) explain why a smaller ΔT can induce CICR at a higher ambient temperature (Fig. 5B). Here, Ca^{2+} outflow is already greater at higher ambient temperature[32,33], and therefore less

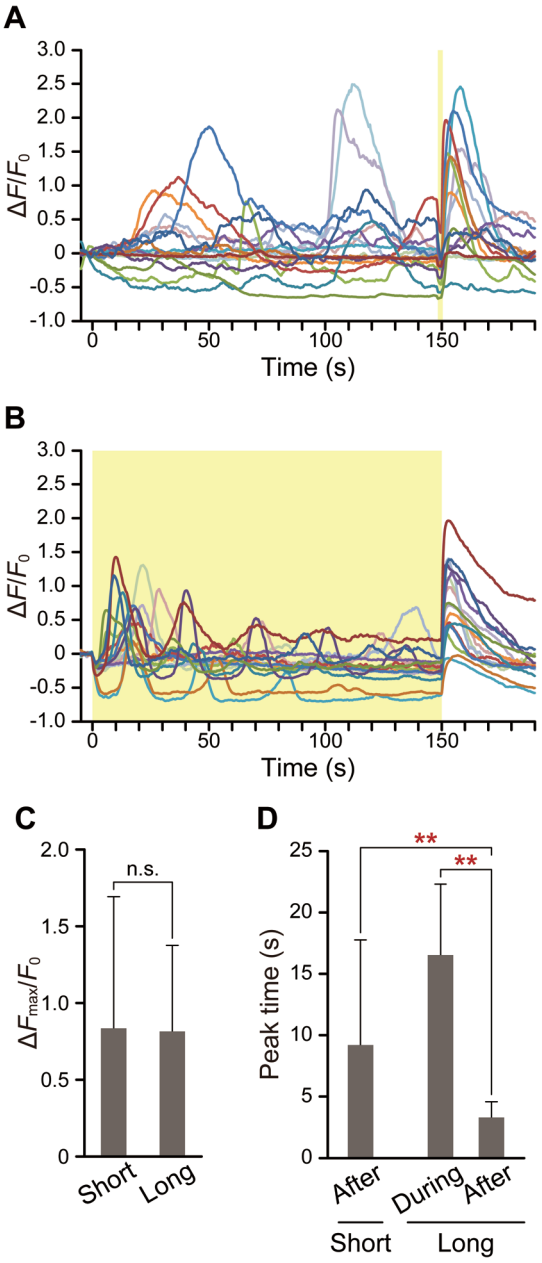

Figure 4 Effect of heating duration on peak time. (A and B) Time course of $\Delta F/F_0$ following short, 2-s (A, n=17 cells) or long, 150-s (B, n=16 cells) heat pulses. The laser power as displayed on the controller was 1.58 W. Yellow areas represent the duration of IR laser irradiation. (C) Effect of heating duration on the peak value of the Ca^{2+} burst that occurred after re-cooling. Mean±standard deviation was calculated from the data shown in (A) and (B) (p=0.82). (D) Comparisons of the time required to reach the peak value of the first Ca^{2+} burst during heating and after re-cooling. Mean±standard deviation was calculated from the data shown in (A) and (B). Two data points that did not have peaks are excluded. $p=1.7\times10^{-3}$ (after the short heat pulse) and $p=3.9\times10^{-6}$ (during the long heat pulse) were determined with respect to the peak time after the long heat pulse. All measurements were performed at 26.5°C. Significant differences are indicated by double asterisks ($p<0.01$). Data at each time point were normalized by the average value from –5 s to 0 s (F_0).

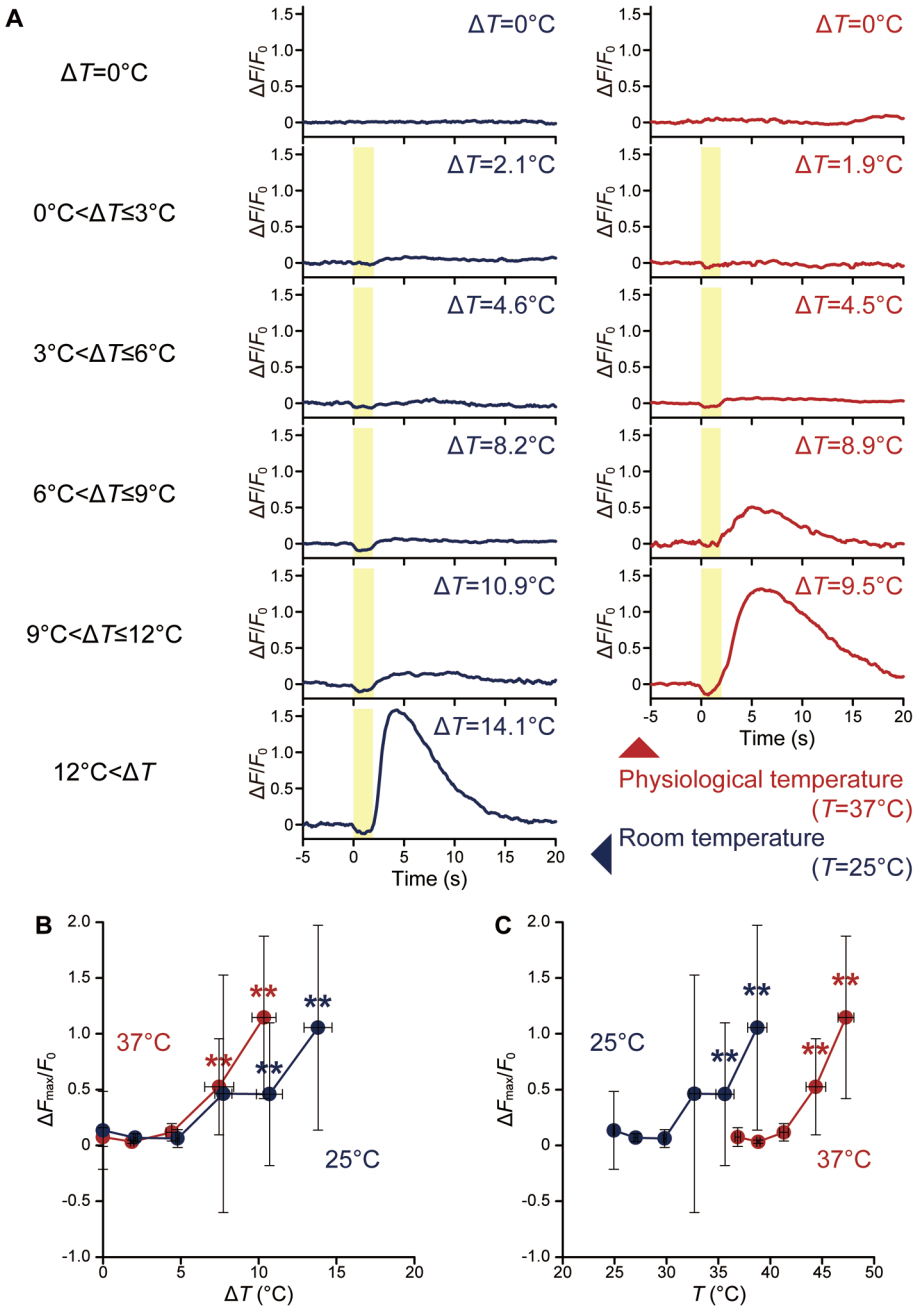

Figure 5 Effect of ambient temperature on thermosensitivity for a short (2 s) heat pulse. (A) Time course of $\Delta F/F_0$ in a cell exposed to various ΔT at room and physiological temperatures (25°C and 37°C, respectively). The duration of irradiation is indicated by the yellow area. (B) Relationship between ΔT and $\Delta F_{max}/F_0$. Plots display mean $\Delta F_{max}/F_0$ for ΔT=0°C, 0°C<ΔT≤3°C, 3°C<ΔT≤6°C, 6°C<ΔT≤9°C, 9°C<ΔT≤12°C, and 12°C<ΔT. (C) Relationship between T (=ambient temperature+ΔT) and $\Delta F_{max}/F_0$. Plots and curves at 25°C (n=58 cells) and 37°C (n=57 cells) are shown in blue and red, respectively. Error bars represent the standard deviation of the $\Delta F_{max}/F_0$ and ΔT (B) or T (C). Significant differences against ΔT=0°C are indicated by double asterisks (p<0.01). Individual plots are shown in Supplementary Figure S3. Data at each time point were normalized by the average value for 5 s before heating (F_0).

additional, heat pulse-induced Ca^{2+} outflow is required to attain the threshold $[Ca^{2+}]_{cyt}$ for CICR. (iv) Excess $[Ca^{2+}]_{cyt}$ then activates SERCA[28,29] and shifts IP_3R to the closed state[30,31], so that $[Ca^{2+}]_{cyt}$ begins to return to the original level (v), which is followed by a damping of $[Ca^{2+}]_{cyt}$ oscillations probably via mitochondrial Ca^{2+} influx[34]. (vi)–(viii) After the re-cooling step following the long heat pulse, steps (iii)–(v) described for the short heat pulse take place. The idea that Ca^{2+} bursts after re-cooling have the same molecular mechanisms regardless of heat pulse duration for the same ΔT is supported by the present data (Fig. 4C). However, peak times for short and long heat pulses after re-cooling differed

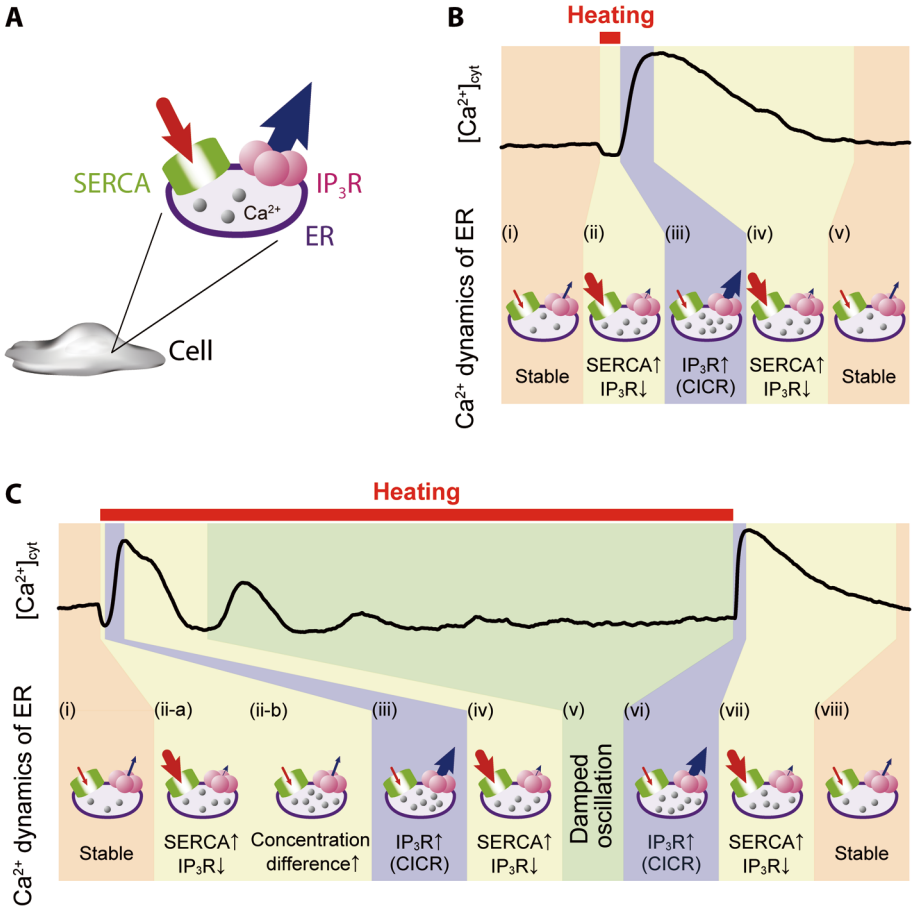

Figure 6 A heat pulse-induced Ca^{2+} burst caused by an imbalance of Ca^{2+} flow through ER membrane. (A) Schematic of ER depicting Ca^{2+} flow from cytoplasm to ER via SERCA (red arrow) and from ER to cytoplasm through IP_3R (blue arrow). (B and C) Representative time courses of cytoplasmic Ca^{2+} dynamics shown in Figure 4A (short heat pulse) and B (long heat pulse). The thickness of the arrow indicates the relative amount of Ca^{2+} flow, which is determined not only by the temperature dependence of SERCA and IP_3R but also by the CICR mechanism and the difference in Ca^{2+} concentrations between cytoplasm and ER.

significantly (Fig. 4D). This difference is consistent with the observation that a smaller ΔT can induce CICR at higher ambient temperatures (Fig. 5B) as the identical scenario discussed above in (ii-b) and (iii) can explain both results; i.e., the larger outflow of Ca^{2+} from ER to cytoplasm through IP_3R at higher ambient temperatures is easier to reach the threshold of CICR.

In this study 2-APB and heparin were used as inhibitors of IP_3R. 2-APB is known to also inhibit TRPM8 located at ER[35]. Our results in Figure 2H showed cells responded when cells were treated with lower concentrations of 2-APB (half maximal inhibitory concentration (IC_{50}) of 83 μM). The lower concentrations used are below the known range of IP_3R inhibition (IC_{50} of 42 μM in the presence of 100 nM IP_3)[36] but within the known range of TRPM8 inhibition (IC_{50} of 1.66–4.9 μM in the presence of 500 μM menthol)[35,37]. We showed that cells injected with heparin responded significantly less than injection control (Fig. 2G), while heparin does not affect TRPM8[38]. It was reported that the open probability of TRPM8 is higher below ~25°C[1,39–41], i.e., TRPM8 is probably inactive in the range of the temperature of this study. Thus, our results strongly suggest that IP_3R and SERCA, but not TRPM8, are responsible for the current heat pulse-induced Ca^{2+} dynamics.

Wei *et al.* showed that Ca^{2+} flickers consisted of high $[Ca^{2+}]_{cyt}$ microdomains in WI-38 fibroblasts, and cell migration was steered by Ca^{2+} flickers[26]. In the present study, we have demonstrated that $[Ca^{2+}]_{cyt}$ dynamics are controlled, that is, Ca^{2+} burst can be induced at any timings by applying a local heat pulse. Thus, our results suggest the possibility that cell functions including migration which is regulated by intracellular Ca^{2+} dynamics, can be controlled by spatio-temporally altering temperature.

Acknowledgements

This research was supported by the Grants-in-Aid for Specially Promoted Research and Scientific Research (S) (to SI), Young Scientist (A) (to KO and MS), Challenging Exploratory Research (to KO and MS), and the Grant for

Excellent Graduate Schools (to HI) from the Ministry of Education, Culture, Sports, Science and Technology of Japan. The funders had no role in study design, data collection and analysis, decision to publish, or preparation of the manuscript.

The authors thank Prof. L. Orban (Temasek Life Sciences Laboratory Limited, Singapore) for critical reading of the manuscript, Ms. T. Arai (Waseda University, Japan) for technical assistance, and reviewers for their valuable comments to improve the manuscript.

References

1. Clapham, D. E. TRP channels as cellular sensors. *Nature* **426**, 517–524 (2003).
2. Protasi, F., Shtifman, A., Julian, F. J. & Allen, P. D. All three ryanodine receptor isoforms generate rapid cooling responses in muscle cells. *Am. J. Physiol. Cell Physiol.* **286**, C662–670 (2004).
3. Stavermann, M., Buddrus, K., St John, J. A., Ekberg, J. A. K., Nilius, B., Deitmer, J. W. & Lohr, C. Temperature-dependent calcium-induced calcium release via $InsP_3$ receptors in mouse olfactory ensheathing glial cells. *Cell Calcium* **52**, 113–123 (2012).
4. Sitsapesan, R., Montgomery, R. A., MacLeod, K. T. & Williams, A. J. Sheep cardiac sarcoplasmic reticulum calcium-release channels: modification of conductance and gating by temperature. *J. Physiol.* **434**, 469–488 (1991).
5. Dickinson, G. D. & Parker, I. Temperature dependence of IP_3-mediated local and global Ca^{2+} signals. *Biophys. J.* **104**, 386–395 (2013).
6. Tseeb, V., Suzuki, M., Oyama, K., Iwai, K. & Ishiwata, S. Highly thermosensitive Ca^{2+} dynamics in a HeLa cell through IP_3 receptors. *HFSP J.* **3**, 117–123 (2009).
7. Dode, L., Van Baelen, K., Wuytack, F. & Dean, W. L. Low temperature molecular adaptation of the skeletal muscle sarco(endo)plasmic reticulum Ca^{2+}-ATPase 1 (SERCA 1) in the wood frog (*Rana sylvatica*). *J. Biol. Chem.* **276**, 3911–3919 (2001).
8. Tsutsumi, M., Kumamoto, J. & Denda, M. Intracellular calcium response to high temperature is similar in undifferentiated and differentiated cultured human keratinocytes. *Exp. Dermatol.* **20**, 839–840 (2011).
9. Teets, N. M., Yi, S., Lee, R. E. & Denlinger, D. L. Calcium signaling mediates cold sensing in insect tissues. *Proc. Natl. Acad. Sci. USA* **110**, 9154–9159 (2013).
10. Hayflick, L. The limited *in vitro* lifetime of human diploid cell strains. *Exp. Cell Res.* **37**, 614–636 (1965).
11. Ungerstedt, J. S., Sowa, Y., Xu, W.-S., Shao, Y., Dokmanovic, M., Perez, G., Ngo, L., Holmgren, A., Jiang, X. & Marks, P. A. Role of thioredoxin in the response of normal and transformed cells to histone deacetylase inhibitors. *Proc. Natl. Acad. Sci. USA* **102**, 673–678 (2005).
12. Kim, J. S., Song, K. S., Joo, H. J., Lee, J. H. & Yu, I. J. Determination of cytotoxicity attributed to multiwall carbon nanotubes (MWCNT) in normal human embryonic lung cell (WI-38) line. *J. Toxicol. Environ. Health. A* **73**, 1521–1529 (2010).
13. Sugarman, B. J., Aggarwal, B. B., Hass, P. E., Figari, I. S., Palladino, M. A. Jr. & Shepard, H. M. Recombinant human tumor necrosis factor-α: effects on proliferation of normal and transformed cells in vitro. *Science* **230**, 943–945 (1985).
14. Oyama, K., Mizuno, A., Shintani, S. A., Itoh, H., Serizawa, T., Fukuda, N., Suzuki, M. & Ishiwata, S. Microscopic heat pulses induce contraction of cardiomyocytes without calcium transients. *Biochem. Biophys. Res. Commun.* **417**, 607–612 (2012).
15. Kamei, Y., Suzuki, M., Watanabe, K., Fujimori, K., Kawasaki, T., Deguchi, T., Yoneda, Y., Todo, T., Takagi, S., Funatsu, T. & Yuba, S. Infrared laser-mediated gene induction in targeted single cells *in vivo*. *Nat. Methods* **6**, 79–81 (2009).
16. Zeeb, V., Suzuki, M. & Ishiwata, S. A novel method of thermal activation and temperature measurement in the microscopic region around single living cells. *J. Neurosci. Methods* **139**, 69–77 (2004).
17. Kolodner, P. & Tyson, A. J. Microscopic fluorescent imaging of surface temperature profiles with 0.01°C resolution. *Appl. Phys. Lett.* **40**, 782–784 (1982).
18. Koval, M. Sharing signals: connecting lung epithelial cells with gap junction channels. *Am. J. Physiol. Lung Cell. Mol. Physiol.* **283**, L875–L893 (2002).
19. Haydon, P. G. GLIA: listening and talking to the synapse. *Nat. Rev. Neurosci.* **2**, 185–193 (2001).
20. Radu, A., Dahl, G. & Loewenstein, W. R. Hormonal regulation of cell junction permeability: Upregulation by catecholamine and prostaglandin E_1. *J. Membr. Biol.* **70**, 239–251 (1982).
21. Maloney, J. A., Tsygankova, O. M., Yang, L., Li, Q., Szot, A., Baysal, K. & Williamson, J. R. Activation of ERK by Ca^{2+} store depletion in rat liver epithelial cells. *Am. J. Physiol.* **276**, C221–230 (1999).
22. Woodruff, M. L., Sampath, A. P., Matthews, H. R., Krasnoperova, N. V., Lem, J. & Fain, G. L. Measurement of cytoplasmic calcium concentration in the rods of wild-type and transducin knock-out mice. *J. Physiol.* **542**, 843–854 (2002).
23. Oliver, A. E., Baker, G. A., Fugate, R. D., Tablin, F. & Crowe, J. H. Effects of temperature on calcium-sensitive fluorescent probes. *Biophys. J.* **78**, 2116–2126 (2000).
24. Oyama, K., Takabayashi, M., Takei, Y., Arai, S., Takeoka, S., Ishiwata, S. & Suzuki, M. Walking nanothermometers: spatio-temporal temperature measurement of transported acidic organelles in single living cells. *Lab Chip* **12**, 1591–1593 (2012).
25. Takei, Y., Arai, S., Murata, A., Takabayashi, M., Oyama, K., Ishiwata, S., Takeoka, S. & Suzuki, M. A nanoparticle-based ratiometric and self-calibrated fluorescent thermometer for single living cells. *ACS Nano* **8**, 198–206 (2014).
26. Wei, C., Wang, X., Chen, M., Ouyang, K., Song, L. S. & Cheng, H. Calcium flickers steer cell migration. *Nature* **457**, 901–905 (2009).
27. Usachev, Y. M. & Thayer, S. A. All-or-none Ca^{2+} release from intracellular stores triggered by Ca^{2+} influx through voltage-gated Ca^{2+} channels in rat sensory neurons. *J. Neurosci.* **17**, 7404–7414 (1997).
28. Satoh, K., Matsu-ura, T., Enomoto, M., Nakamura, H., Michikawa, T. & Mikoshiba, K. Highly cooperative dependence of sarco/endoplasmic reticulum calcium ATPase (SERCA) 2a pump activity on cytosolic calcium in living cells. *J. Biol. Chem.* **286**, 20591–20599 (2011).
29. Lytton, J., Westlin, M., Burk, S. E., Shull, G. E. & MacLennan, D. H. Functional comparisons between isoforms of the sarcoplasmic or endoplasmic reticulum family of calcium pumps. *J. Biol. Chem.* **267**, 14483–14489 (1992).
30. Bezprozvanny, I., Watras, J. & Ehrlich, B. E. Bell-shaped calcium-response curves of $Ins(1,4,5)P_3$- and calcium-gated channels from endoplasmic reticulum of cerebellum. *Nature* **351**, 751–754 (1991).
31. Shinohara, T., Michikawa, T., Enomoto, M., Goto, J., Iwai, M., Matsu-ura, T., Yamazaki, H., Miyamoto, A., Suzuki, A. & Mikoshiba, K. Mechanistic basis of bell-shaped dependence of inositol 1,4,5-trisphosphate receptor gating on cytosolic

calcium. *Proc. Natl. Acad. Sci. USA* **108**, 15486–15491 (2011).
32. Barrero, M. J., Montero, M. & Alvarez, J. Dynamics of [Ca^{2+}] in the Endoplasmic Reticulum and Cytoplasm of Intact HeLa Cells. *J. Biol. Chem.* **272**, 27694–27699 (1997).
33. Montero, M., Barrero, M. J. & Alvarez, J. [Ca^{2+}] microdomains control agonist-induced Ca^{2+} release in intact HeLa cells. *FASEB J.* **11**, 881–885 (1997).
34. Ishii, K., Hirose, K. & Iino, M. Ca^{2+} shuttling between endoplasmic reticulum and mitochondria underlying Ca^{2+} oscillations. *EMBO Rep.* **7**, 390–396 (2006).
35. Acharya, S. A, Portman, A., Salazar, C. S. & Schmidt, J. J. Hydrogel-stabilized droplet bilayers for high speed solution exchange. *Sci. Rep.* **3**, 3139 (2013).
36. Maruyama, T., Kanaji, T., Nakade, S., Kanno, T. & Mikoshiba, K. 2APB, 2-aminoethoxydiphenyl borate, a membrane-penetrable modulator of Ins(1,4,5)P_3-induced Ca^{2+} release. *J. Biochem.* **122**, 498–505 (1997).
37. El-Arabi, A. M., Salazar, C. S. & Schmidt, J. J. Ion channel drug potency assay with an artificial bilayer chip. *Lab Chip* **12**, 2409–2413 (2012).
38. Thebault, S., Lemonnier, L., Bidaux, G., Flourakis, M., Bavencoffe, A., Gordienko, D., Roudbaraki, M., Delcourt, P., Panchin, Y., Shuba, Y., Skryma, R. & Prevarskaya, N. Novel role of cold/menthol-sensitive transient receptor potential melastatine family member 8 (TRPM8) in the activation of store-operated channels in LNCaP human prostate cancer epithelial cells. *J. Biol. Chem.* **280**, 39423–39435 (2005).
39. McKemy, D. D., Neuhausser, W. M. & Julius, D. Identification of a cold receptor reveals a general role for TRP channels in thermosensation. *Nature* **416**, 52–58 (2002).
40. Peier, A. M., Moqrich, A., Hergarden, A. C., Reeve, A. J., Andersson, D. A., Story, G. M., Earley, T. J., Dragoni, I., Mclntyre, P., Bevan, S. & Patapoutian, A. A TRP channel that senses cold stimuli and menthol. *Cell* **108**, 705–715 (2002).
41. Cao, C., Yudin, Y., Bikard, Y., Chen, W., Liu, T., Li, H., Jendrossek, D., Cohen, A., Pavlov, E., Rohacs, T. & Zakharian, E. Polyester Modification of the Mammalian TRPM8 Channel Protein: Implications for Structure and Function. *Cell Rep.* **4**, 302–315 (2013).